Electronic Supplementary Material (ESI) for Integrative Biology.

Supplementary Materials

Supplementary Information

1. Modelling pressure equilibration through bypass channel

A central feature of the microfluidic migration device is a low fluid resistance bypass channel, whose purpose is to quickly equilibrate differences in fluid levels between the source and sink reservoirs and thus facilitate formation of a diffusion-based gradient. To assess the efficiency of the bypass channel, we computed the fluid flow through the constriction channels and the bypass channel, and the time required for differences in the fluid levels of the reservoirs to equilibrate in the absence and presence of a bypass channel. For low Reynolds numbers, as found in most microfluidic system, the volumetric flow rate, *Q,* through a given channel is determined by the pressure difference across the channel, *Δp,* and the hydrodynamic resistance, *R*.

$$Q = \frac{\Delta p}{R} \tag{1}$$

For the fluid flow between the reservoirs, the pressure difference arises from the difference in fluid levels, Δ*h*. Thus, the volume flow rate can be expressed as

$$Q = \frac{\rho g \Delta h}{R} \tag{2}$$

where *ρ* denotes the density of water (medium), *g* the gravitational acceleration, and *R* the overall resistance of the microfluidic system, including the resistance of the bypass channel and the constriction channels. As fluid flows from one reservoir into the other, the height difference Δh changes at a rate depending on the exchanged volume, *Q*, and the cross-sectional area of the reservoir, *A*.

$$\frac{d\Delta h}{dt} = -\frac{2\rho g \Delta h}{AR} = \frac{2\rho g}{AR}\Delta h \tag{3}$$

The factor '2' reflects the fact that as fluid volume is exchanged between the reservoirs, one reservoir increases in height, whereas the height of the other reservoir decreases by the same amount. The negative sign indicates that the height difference decreases over time. The solution to this simple differential equation is given by

$$\Delta h(t) = \Delta h_0 e^{-\frac{2\rho g}{AR}t} \tag{4}$$

where Δh_0 indicates the initial height difference between the reservoirs. This can be expressed in short form using the characteristic time constant τ:

$$\Delta h(t) = \Delta h_0 e^{-\frac{t}{\tau}} \tag{5}$$

and

$$\tau = \frac{AR}{2\rho g} \tag{6}$$

Equations (5) and (6) can be used to compute the time required for the two reservoirs to equilibrate their fluid levels, given the device-specific cross-sectional areas of the reservoirs, *A*, the hydrodynamic resistance of a particular device, and the initial difference in fluid levels, Δh_0. Furthermore, substituting equation (5) into equation (3) yields an expression for the volume flow rate at a given time:

$$Q(t) = \frac{\rho g \Delta h_0}{R} e^{-\frac{2\rho g}{AR}t} \tag{7}$$

The total exchanged fluid volume, V, can then be determined by integrating equation (8) over time:

$$V(t) = \int_0^t Q(t)dt \tag{8}$$

Integration of equation (9) yields the following expression:

$$V(t) = \frac{\Delta h_0 A}{2}\left(1 - e^{-\frac{2\rho g}{AR}t}\right) \tag{9}$$

The cross-sectional area of each reservoir can be easily determined based on the diameter of the hole-punch (i.e., 6 mm). The hydrodynamic resistance, R, of a microfluidic channel at low Reynolds numbers is given by equation (11),[29] where l is the length of the channel, w is the width of the channel, h the height of the channel, and μ is the viscosity of the fluid.

$$R = \frac{12l\mu}{wh^3\left[1 - \frac{192\,h}{\pi^5\,w}tanh\left(\frac{\pi w}{2h}\right)\right]} \tag{10}$$

For aspect ratios with $w > h$, equation (11) can be approximated by the following expression.

$$R = \frac{12l\mu}{wh^3\left[1 - 0.63\frac{h}{w}\right]} \tag{11}$$

Equations (11) and (12) can be directly used to compute the resistance of the bypass channel (l = 9.313 mm; w = 1.0 mm; h = 250 µm), ρ = 9.934 kg/m^3 for the density of water at 37 °C and μ = 0.00069 N s/m^2 as the viscosity of water at 37 °C. Given those parameters, the hydrodynamic resistance of the bypass channel is R_{bypass} = 5.86 × 10^9 N s/m^5. The resistance of the constriction channels can be approximated as a combination of shorter segments in series and in parallel, with the geometries of the individual segments defined by the constriction channel geometry. For a number of channels in series, the total resistance R_{total_series} is given as the sum of the individual constrictions with resistance R_i:

$$R_{total\_series} = \sum R_i \tag{12}$$

In contrast, for channels arranged in parallel, the total resistance $R_{total\_parallel}$ is given as the reciprocal sum of the inverse of the individual constrictions with resistance R_i:

$$\frac{1}{R_{total\_parallel}} = \sum \frac{1}{R_i} \tag{13}$$

The particular device modelled here had the following geometries: 250 µm tall collection areas with a width of 2.61 mm and length of 1.11 mm located before and after the constriction areas; 66 parallel constriction channels with a height of 5 µm, length of 280 µm, and width ranging from 15 µm down to 2 µm in the narrowest constrictions, along with 21 wider (15 µm) channels also 5 µm in height and 280 µm in length. The combined resistance of this microfluidic segment was computed to be $R_{channels}$ = 1.43 × 10^{13} N s/m^5. Since the bypass channel and constriction channels are arranged in parallel, the total resistance of the device can be determined using equation (13) and then be used to compute the equilibration time using equation (6). Similarly, as the same pressure difference is applied to the bypass channel and the constriction channels, the fluid flow through each of the systems can be computed based on equation (9). The results of this modelling approach are given in Supplementary Tables 1 and 2, and Supplementary Figure 1.

2. Modelling gradient formation across constriction channels

For an initial order-of-magnitude estimate of the time required to form a steady-state gradient across the constriction channels of the device, we modelled the diffusion as a 1-D random walk. The root-mean-square displacement of a given molecule is thus defined as:

$$X_{rms} = \sqrt{2Dt} \quad (14)$$

where X_{rms} is the root-mean-square displacement, D is the diffusion coefficient or diffusivity of the molecule in the fluid of interest and t is time. The diffusivity of PDGF in water was selected as $D_{PDGF} = 1.13 \times 10^{-10}$ m^2/s, and the diffusivity for 70 kDa dextran as $D_{70kDa\text{-}dextran} = 2.31 \times 10^{-11}$ m^2/s, based on its molecular weight.[30, 31]

For a more detailed analysis of gradient formation, we performed finite element analysis that incorporated the exact channel geometry of the devices using COMSOL software (COMSOL, Inc., Burlington, MA). We modelled the diffusion of 70 kDa dextran for the initial simulations and validation, because the results of the computational model could be compared to data from experiments in which we measured the fluorescence intensity of Texas Red-labelled 70 kDa dextran introduced into the source reservoir of the device and imaged inside the constriction channels over time. After establishing the accuracy of the COMSOL model (Fig. 2), we carried out additional computational studies comparing the gradient formation in the two-layer device with a single-layer (5 μm tall channels only) version, and also comparing the times required to form a stable gradient when using PDGF vs. 70 kDa dextran. Results of the computation model were analysed by investigating the concentration profiles across the constriction channels and the 15 μm wide channels. Time to achieve a steady-state profile was determined by analysing the concentration in the centre of the constriction channels, half-way between the sink and the source reservoir at the site of the second constriction inside the channel. Since the chemoattractant concentration at a particular point in the device will asymptotically approach its steady-state concentration, we compared the time needed to reach 90% and 95% of the steady-state concentration for PDGFand 70 kDa dextran molecules. The results from these calculations are given in Supplementary Figure 3c.

3. Modelling the diffusion of the PDGF across the bypass channel

To assess whether diffusion through the large bypass channel could result in rapid equilibration of the concentrations between the sink and source reservoirs, we calculated the diffusion rate of a typical chemoattractant (i.e., platelet derived growth factor, PDGF) across the length of the bypass channel and through the constrictions, using Fick's law.

The device measurements were as follows:

Bypass channel dimensions:

- Length: 9313 μm
- Width: 1000 μm
- Height: 250 μm
- Cross-section: 2.5×10^5 μm^2 = 2.5×10^{-7} m^2

Constrictions:

- Length: 280 μm
- Width: 2610 μm
- Height: 5 μm
- Cross-section:
    - Without constrictions: $2610 \times 5 = 1.3 \times 10^4$ μm^2 = 1.3×10^{-8} m^2
    - Assuming 66 channels 2 μm wide and 21 channels 15 μm wide: $(66 \times 2 + 21 \times 15) \times 5 = 2235$ μm^2 = 2.235×10^{-9} m^2

Reservoir:

- Height: 5 mm
- Diameter: 5 mm
- Volume: $\pi \times (5/2)^2 \times 5 = 98\ mm^3 = 9.8 \times 10^{-8}\ m^3$

Other important values:
- Diffusion constant of PDGF: $1.13 \times 10^{-10}\ m^2/s$
- Time between change of cell culture medium: 24 hours = 86400 s
- Initial concentration in source: 200 ng/ml = 2×10^{-7}g/ml = 2×10^{-4} g/l = 2×10^{-4} g/dm^3 = 2×10^{-1} g/m^3

We first computed the amount of solute that diffused across the length of the bypass channel from the source to the sink reservoir within 24 hours.

Given Fick's law:

$$J = -D\frac{\partial C}{\partial x} = \frac{m}{A \times t} \quad (15)$$

i.e., $$m = -D\frac{\Delta C}{\Delta x}At = -2.825 \times 10^{-17}\frac{\Delta C}{\Delta x}t\ [m^4/s] \quad (16)$$

Using a conservative estimate that the concentrations at the sink and source remain constant (i.e., 200 ng/mL and 0 ng/mL, respectively), i.e., that the mass transfer is maintained at the maximum diffusive flux between the source and the sink, and looking at the resulting mass transfer over 24 hours, we obtain the following:

$$m = \frac{-2.825 \times 10^{-17} \times 8.64 \times 10^4}{9.313 \times 10^{-3}} \times 2 \times 10^{-1} = 5.24 \times 10^{-11} g \quad (17)$$

Thus, the amount of PDGF exchanged, along the bypass channel, given our initial assumptions, is 5.24×10^{-11}g. Knowing the approximate dimensions of the sink and source reservoirs, we can calculated the amount of PDGF present initially.

$$m = C \times V = 9.8 \times 10^{-8} \times 2 \times 10^{-1} = 1.96 \times 10^{-8} g \quad (18)$$

We can thus say that the proportion of PDGF exchanged across the bypass channel over 24 hours is:

$$m(\%) = \frac{m(exchanged\ over\ 24\ hours)}{m(initial\ in\ source\ reservoir)} = \frac{5.24 \times 10^{-11}}{1.96 \times 10^{-8}} = 0.267\ \%$$

Thus, the amount of solute exchanged across the bypass channels is less than a percent. This minuscule change in concentration, even assuming a maximal diffusive flux of the solute, supports our above assumption that the sink and source concentrations remain virtually constant in-between medium changes (every 24 hours).

We next modelled the amount of solute that diffused through the constriction channels. To do this, we again used Fick's law and modelled the cross-sectional area of the constriction channels in two different ways. First we modelled the constriction channels as an open channel 2610 µm wide and 5 µm tall (cross section 1.3×10^{-5} m^2), i.e. with a larger cross-sectional area than the actual constriction channels, again deciding to use a conservative approach and err on the side of increased mass transfer. Second, we modelled the constriction channels as a series of 66 channels 2 µm wide and 21 channels 15 µm wide (cross-section 2.235×10^{-6} m^2), i.e. the smallest cross-sectional area in the constriction channels.

Open channel:

$$m = -D\frac{\Delta C}{\Delta x}At = -1.13 \times 10^{-10} \times \frac{-1.47 \times 10^{-15}}{2.8 \times 10^{-4}} \times 1.3 \times 10^{-5} \times 8.64 \times 10^4 = 9.07 \times 10^{-11} g$$

, i.e., **0.46%**

Series of channels:

$$m = -D\frac{\Delta C}{\Delta x}At = -1.13 \times 10^{-10} \times \frac{-1.47 \times 10^{-15}}{2.8 \times 10^{-4}} \times 2.235 \times 10^{-6} \times 8.64 \times 10^{4} = 1.56 \times 10^{-11} g$$

, i.e. **0.08%**

The amount of PDGF that diffuses through the constrictions is thus on the order of 0.1% to 0.5%, i.e. similar to the amount of PDGF that diffuses across the bypass channel. These values are very small compared to the amount of PDGF present in the reservoirs at the beginning of the experiment and the PDGF diffusion can thus be considered to be negligible during a typical experiment in which the cell culture medium is changed every 24 hours.

Supplementary Tables

	Constriction channels only	Bypass channel only	Constriction channels and bypass channel
Resistance ($N*s/m^5$)	4.5440×10^{13}	5.8566×10^{9}	5.8559×10^{9}
Equilibration time constant	45274 s (12.58 h)	5.841 s	5.840 s

Supplementary Table 1. **Hydrodynamic resistance and equilibration time constants for a microfluidic device containing only constriction channels or constriction channels and a larger bypass channel to promote fluid level equilibration between the reservoirs**. We considered fluid level differences of 0.25, 0.5 and 1.0 mm, corresponding to overfilling one of the reservoirs by 5%, 10% or 20%, respectively. Based on the typical device geometry, we calculated the total hydrodynamic resistance of the constriction channels, including the resistance of the 250 µm tall collection area leading up to the mouth of the constrictions, and of the bypass channel. The resistance of the bypass channel was four orders of magnitude lower than the resistance of the parallel constriction channels, so that the combined fluidic resistance of the bypass channel and the constriction channels is dominated by the resistance of the bypass channel.

Equilibration between fluid levels in reservoir	**Initial fluid level difference Δh_0**		
	0.25 mm	**0.5 mm**	**1.0 mm**
Excess volume in one reservoir	4.909 µL	9.817 µL	19.635 µL
Time *T* to equilibrate levels to 1 µm without bypass	69.4 hours	78.2 hours	86.9 hours
Time *T* to equilibrate levels to 1 µm with bypass	32.2 seconds	36.3 seconds	40.3 seconds
Volume exchange completed by t = *T*	99.6%	99.8%	99.9%
Total volume exchanged*	2.44455 µL	4.89892 µL	9.80766 µL
Volume exchanged through bypass channel	2.44424 µL	4.49829 µL	9.80639 µL
Volume exchanged through constrictions channels	0.00032 µL	0.00063 µL	0.00127 µL
Percentage of constriction channel volume displaced	19.37%	38.81%	77.70%

Supplementary Table 2: Effect of bypass channel on fluid level equilibration. Results from modelling the fluid exchange during equilibration in case of initial differences in the fluid levels between the two reservoirs. The excess volumes in the reservoir at initial fluid level differences of 0.25, 0.50, and 1.00 mm correspond to 5%, 10%, or 20% of the nominal volume of a single reservoir (≈98.2 µL), respectively. In the absence of a bypass channel, the entire fluid flow must pass through the constriction channels. In the presence of the bypass channel, the vast majority of the fluid flow will occur through this lower resistance passage, significantly speeding up the equilibration process. *, Please note that the exchanged volume is half of the excess volume, as a decrease in volume in one reservoir results in a corresponding increase in the volume of the other reservoir.

Supplementary Figures

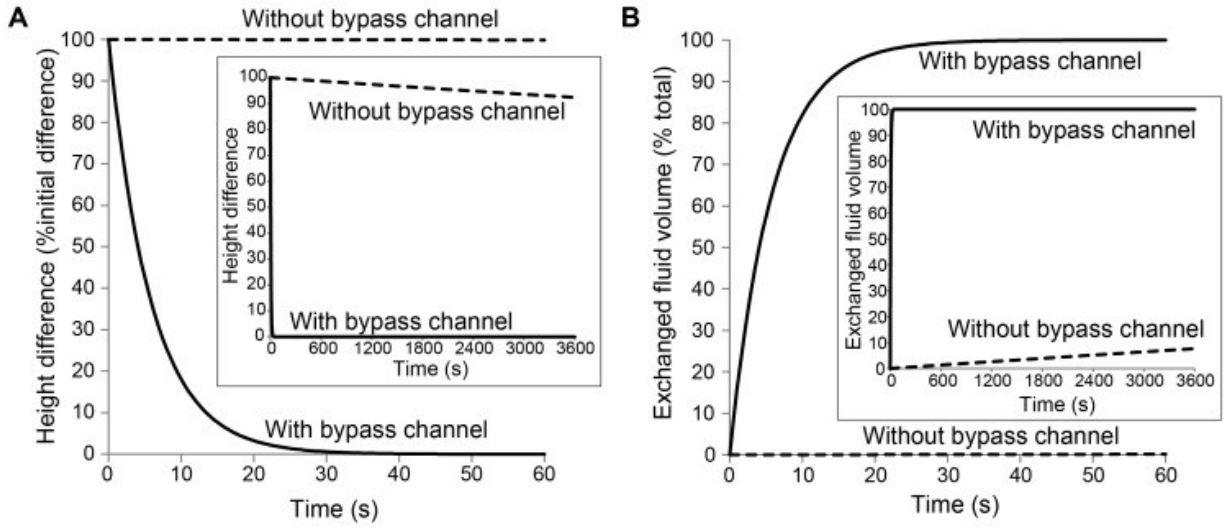

Supplementary Figure 1. Bypass channel accelerates equilibration of fluid levels between reservoirs. (a) Change of the difference in fluid levels, Δh, over time after an initial excess of 9.82 uL in one reservoir, corresponding to 10% overfilling and a height difference of 0.5 mm in the fluid levels between the reservoirs. Results are normalized to the initial difference in fluid levels. With the bypass channel, the fluid levels equilibrate within 36.3 seconds, with equilibration defined as reaching 99.8% (or less than 1 μm height difference) of the final fluid levels. Without the bypass channel, equilibration requires 78.2 hours. Inset depicts the same results plotted with a longer time scale to illustrate the slow equilibration of devices without bypass channels. **(b)** Corresponding results for the fluid volume exchanged between the reservoirs during the equilibration process, expressed as the percentage of the total fluid volume required to level the reservoirs. Inset depicts the same results plotted with longer time scale to illustrate the gradual change over time in devices without a bypass channel.

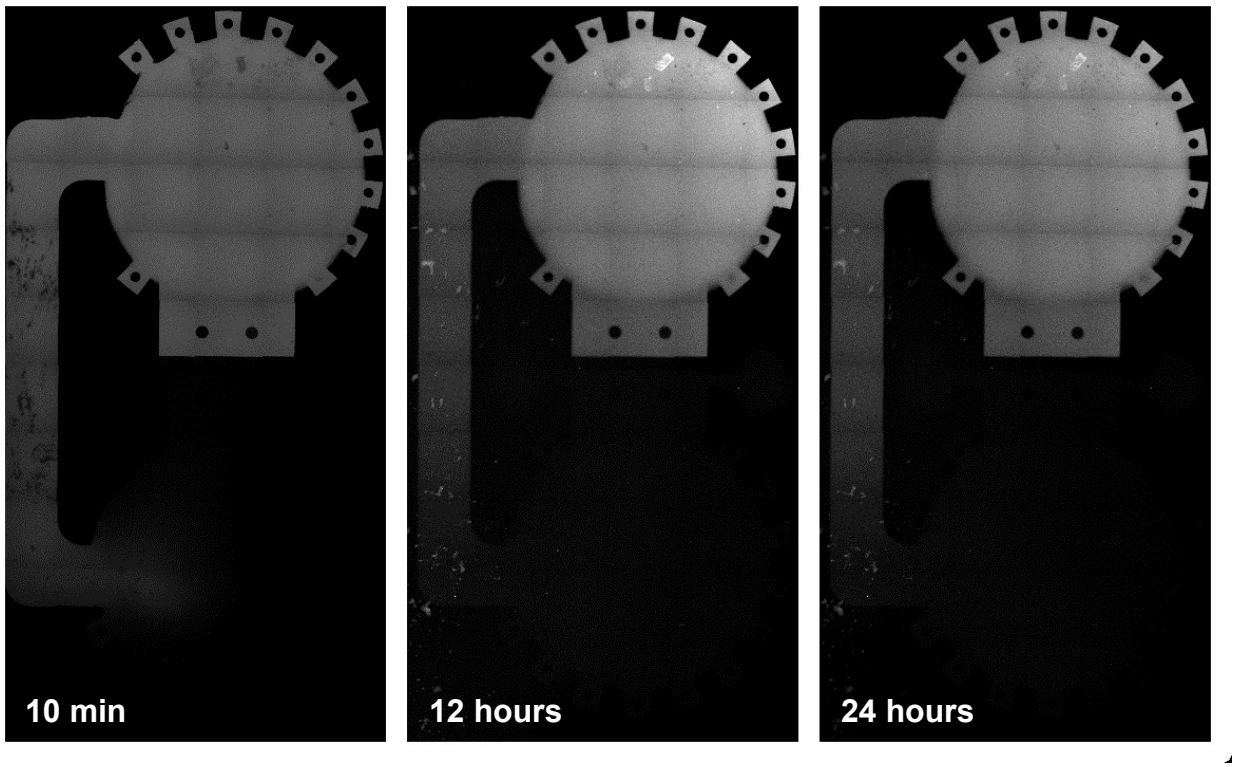

Supplementary Figure 2. Experimental validation of gradient maintenance over 24 hours in the entire device. The device was filled with a solution of PBS with Texas red-conjugated 70 kDa dextran in the source reservoir (top) and PBS in the sink reservoir (bottom). Images were taken using a confocal microscope with a pinhole opening corresponding to a 100 µm stack, at 10 minutes (left), 12 hours (middle) and 24 hours (right), using identical imaging settings. As expected from the modelling calculations, very little equilibration of the fluorescent dye is visible between the sink and source reservoirs, confirming that the sink and source concentrations and thus the gradient remain stable over 24 hours.

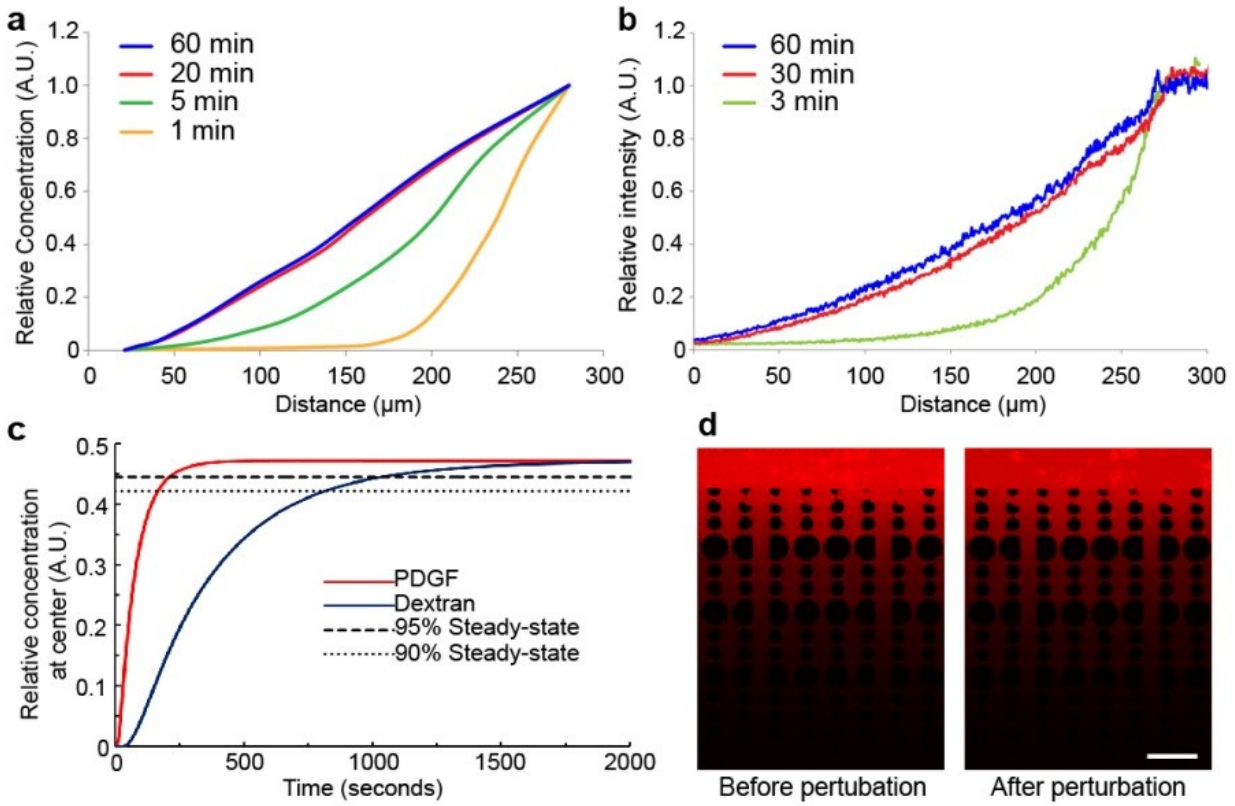

Supplementary Figure 3. Rapid and uniform gradient formation across the constriction channels. **(a)** Modeling the 70 kD dextran gradient using COMSOL software at different time-points. **(b)** Corresponding experimental validation of the gradient formation within minutes of the addition of the dextran-Texas Red, closely matching the modelling results from panel d. **(c)** Results of calculations of the time required to reach a linear gradient (relative concentration of 0.5 at the centre of device) for two different solutes: 70 kD dextran, which was used in the experimental models, and 24 kDa PDGF, which is the chemoattractant used for fibroblasts. The smaller and more diffusive PDGF is predicted to form a stable gradient even more quickly than the larger dextran-Texas Red used in the experimental validation. **(d)** Demonstration of the stability of the diffusion-based gradient to mechanical perturbation the device. Images were taken before (left) and after (right) inverting the device several times, with no detectable difference in the dextran gradient. Scale bar, 50 μm.

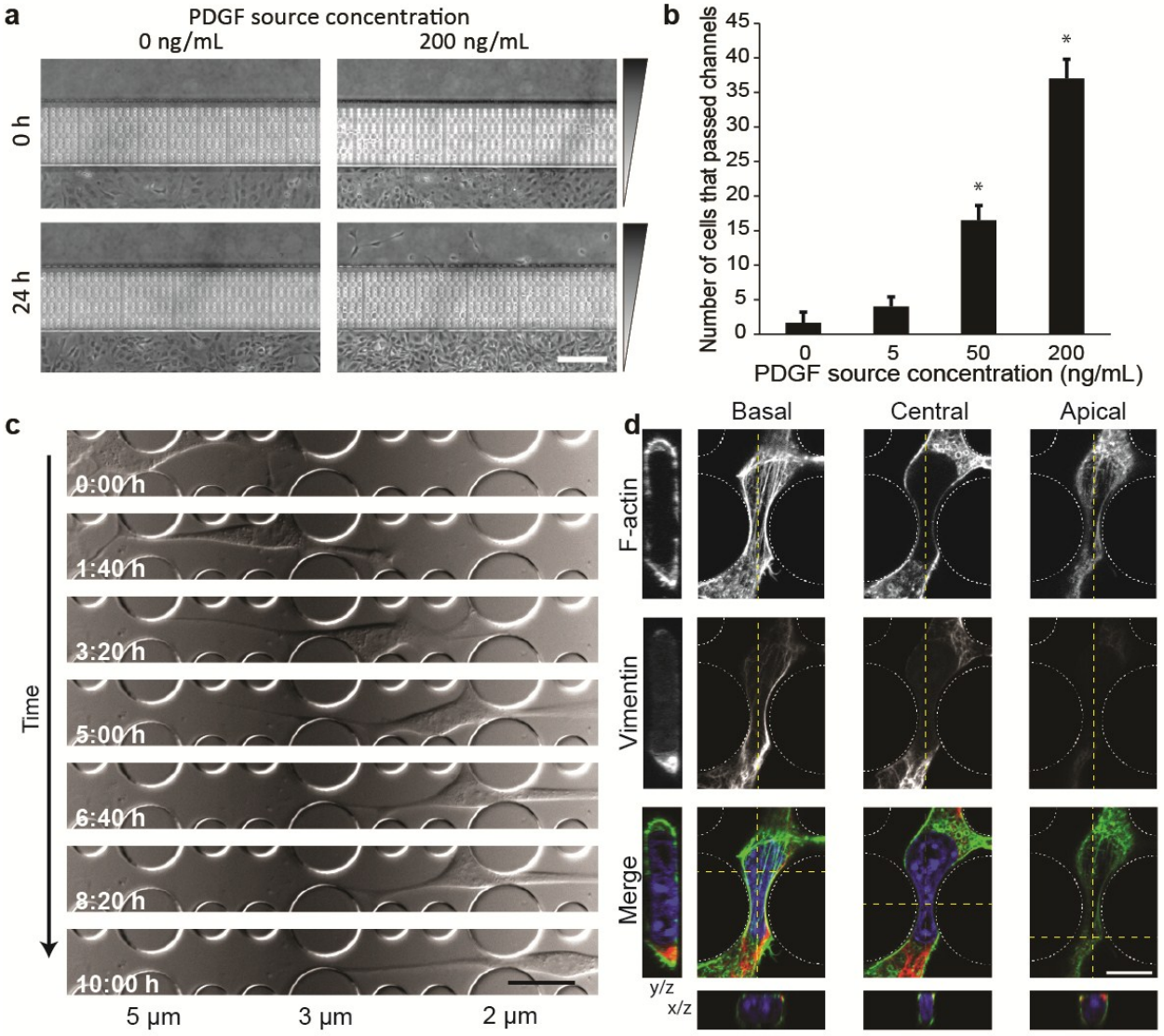

Supplementary Figure 4. Cell migration through the constriction channels. (a) Effect of PDGF chemotactic gradient to stimulate migration of NIH 3T3 fibroblasts through the device. Listed is the maximal PDGF concentration in the source reservoir. Images were taken at the beginning of the experiments and 24 hours later. The number of cells that migrated to the other side of the pillars increased in the presence of the gradient. *, $P < 0.05$ *vs*. control without PDGF. Scale bar, 200 µm. **(b)** Average number of cells that migrated through the devices 24 hours after chemoattractant addition. **(c)** Representative time-lapse image series of a glioblastoma cell migrating through three successive constrictions measuring 5, 3 and 2 µm in width, respectively. Scale bar, 25 µm. See Supplemental Video 2 for corresponding movie. **(d)** High resolution 3-D confocal image stack of an NIH 3T3 fibroblast migrating through a 2 µm-wide constriction. The F-actin (green) network was labelled with phalloidin stain, the vimentin network (red) with an anti-vimentin antibody, and the DNA (blue) with Hoechst 33342 stain. Cross-sections are shown through the basal, central and apical regions of the cell, as well as through the cell along the direction of migration (left) and perpendicular to the direction of migration (right). Scale bar, 10 µm. See Supplemental Video 3 for corresponding movie.

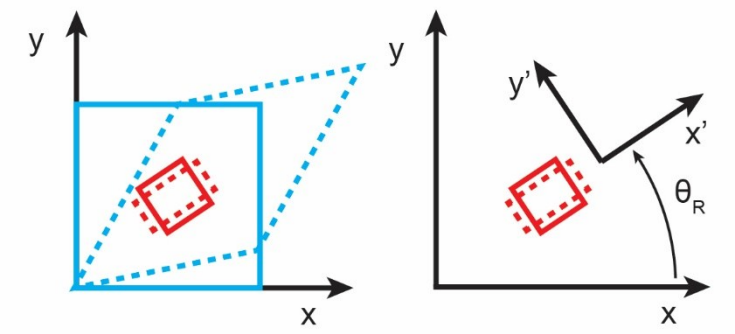

Supplementary Figure 5. Mechanical stress acting on an object (blue outline) will result in it deformation and the distortion of its initial shape (blue dotted outline). The components of the stress and strain tensor experienced by a small volume element within the object are defined by reference frame and the forces acting on the surface of the volume element. Normal stresses act perpendicular on the surface and result in elongation or compression, while shear stresses act parallel to a surface and result in shearing. Rotating the reference frame by an angle θ_R does not change the overall physical forces acting on the volume element and its deformation, but alter the components relative to the surfaces given by the reference frame. For a particular orientation of the reference frame, the shear stress components vanish, leaving only components perpendicular to the surface (red rectangle). These components of the stress and strain tensor at this orientation are defined as the principal stress and strains, respectively, and they represent the maximal and minimal values of the stress/strain. (Figure based on an image obtained at the website Continuum Mechanics [B. McGinty, Principal Stresses & Strains, *Continuum Mechanics*, 2015, http://www.continuummechanics.org].)

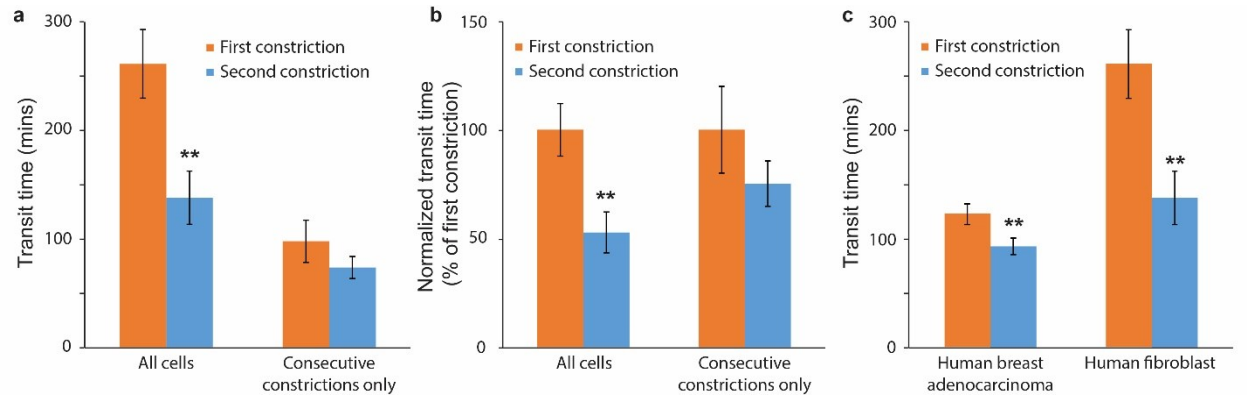

Supplemental Figure 6. Transit time of cells migrating through consecutive 3 × 5 μm² constrictions. (a) Comparison of transit time for human fibroblasts migration through the first (red bar) or second constriction (blue bar) in the microfluidic migration device design depicted on the right in Figure 1g. The data shown is based either on all observed cells (All cells), regardless of whether they cross more than one constriction within the observation period, or based on only cells that migrate through consecutive constrictions within the imaging time frame (Consecutive constrictions only). **, $P < 0.01$ compared to first constriction; $n > 40$ for all cells; $n = 12$ for cells that passed through consecutive constrictions. **(b)** Transit times normalized to the values for the first constriction, using the same data and inclusion criteria as in (a). **, $P < 0.01$ compared to first constriction. **(c)** Transit times of human skin fibroblasts and breast carcinoma cells (MDA-MB-231) for the first and second constriction.

Supplementary Video Legends

Supplementary Video 1. Overview of cells migrating through the migration device. Fibroblasts expressing GFP-lamin A migrate along a chemotactic gradient through three successive constrictions measuring 5 μm, 3 μm and 2 μm in width, respectively. The timestamp is shown in the bottom left corner.

Supplementary Video 2. Glioblastoma cell migrating through three successive constrictions measuring 5 μm, 3 μm and 2 μm in width, respectively. Images from this time-lapse were used in Supplemental Figure 4c. The timestamp is shown in the bottom left corner.

Supplementary Video 3. High resolution 3-D confocal image stack of an NIH 3T3 fibroblast migrating through a 2 μm-wide constriction. Images taken at successive z-positions are shown as a video. Images from this series were used in Supplemental Figure 4d. The z-positions are marked in the top left corner. Scale bar, 5 μm.

Supplementary Video 4. High resolution time-lapse sequence of a fibroblast expressing mCherry-Histone4 (red) and GFP-actin (green) migrating through a 2 μm-wide constriction. Images from this time-lapse series were used in Fig. 3a. The timestamp is shown in the bottom left corner.

Supplementary Video 5. Time-lapse of the nuclear lamina deformation in a human skin fibroblast expressing GFP-prelamin A migrating through a constriction. The outlines of the pillars forming the constrictions are indicated with white circles. Images from this time-lapse series were used in Fig. 3e. The timestamp is shown in the bottom left corner.

Supplementary Video 6. Examples of a time-lapse sequence of the strain values obtained from triangulation of the chromocenters in a wild-type (*Lmna*$^{+/+}$) fibroblast expressing Histone H2B-mNeonGreen. Left, fluorescent images of the cell with triangles used for strain mapping overlaid. Triangle vertices were based on bright chromatin foci (chromocenters). Right, results of the Green-Lagrange strain analysis computed from the change in length of the vertices of each triangle. The color-coded results represent the principal strain values for each of the triangles, based on the eigenvalues of the corresponding strain tensor.

Supplementary Video 7. Examples of a time-lapse sequence of the strain values obtained from triangulation of the chromocenters in a lamin A/C-deficient (*Lmna*$^{-/-}$) fibroblast expressing Histone H2B-mNeonGreen. Left, fluorescent images of the cell with triangles used for strain mapping overlaid. Triangle vertices were based on bright chromatin foci (chromocenters). Right, results of the Green-Lagrange strain analysis computed from the change in length of the vertices of each triangle. The color-coded results represent the principal strain values for each of the triangles, based on the eigenvalues of the corresponding strain tensor.